A. De Gaspari, A. Gilardelli, S. Ricci, A. Airoldi, F. Moens
Design of a Leading Edge Morphing Based on Compliant Structures for a Twin-Prop Regional Aircraft
in: 2018 AIAA/AHS Adaptive Structures Conference - AIAA SciTech, Kissimmee, FL, USA, 8-12 Jan. 2018, ISBN: 9781624105319, p. 1-19, AIAA 2018-1063
doi:10.2514/6.2018-1063

AIAA SciTech Forum
8–12 January 2018, Kissimmee, Florida
2018 AIAA/AHS Adaptive Structures Conference

10.2514/6.2018-1063

Design of a Leading Edge Morphing Based on Compliant Structures for a Twin-Prop Regional Aircraft

A. De Gaspari[1], A. Gilardelli[2], S. Ricci[3] and A. Airoldi[4]
Politecnico di Milano, Department of Aerospace Science and Technology, 20156 Milano, ITALY

F. Moens[5]
ONERA, The French Aerospace Lab, 92190 Meudon, FRANCE

I. Introduction

IN the framework of EU funded Clean Sky 2 REG-IADP AG2 project, one of the activity related to the implementation of morphing concepts focuses on the conceptual design of a morphing Leading Edge able to match the high lift requirements in combination with the adoption of a Natural Laminar Wing. The conceptual design phase includes the definition of the optimal shape as well as the investigation of the possible structural solution in terms of skin, internal compliant structure and possible actuation mechanism.

Morphing Leading Edge is one of the many so-called morphing concepts under investigation since many years. In particular, morphing LE can be included into the most general active camber morphing field, where the main goal is to modify the airfoil camber to increase the aerodynamic performances. The literature reports many and different concepts and applications of this concept, and in the following just a very brief summary is reported, mainly inspired by the huge review activity presented by Friswell in [1].

Boeing around 1973 presented an advanced technology variable-camber wing wind tunnel test in the NASA Ames 14-ft transonic wind tunnel [2]. The wing was equipped with simple hinged leading and trailing-edge flaps but also smooth and curved variable-camber flaps. Large improvements over standard airfoil performance were obtained, but the device was mechanically complex in the wing interior. Starting from the mid-80s, the researchers at Boeing [3][4][5] tried to integrate, on board a military aircraft, a device capable of controlling the wing curvature by means of an automated control system. The first important program in this field, named Advanced Fighter Technology Integration (AFTI)/F-111, was promoted by NASA in collaboration with the USAF. The F-111 wing was modified by adopting six independent sections for the trailing edge (three for each wing, based on sliding panels for the lower surface and flexible panels made of glass fiber for the upper one) and two for the leading edge made of flexible composite; all these surfaces were commanded by electro-hydraulic actuators. Flight tests were conducted on the AFTI/F-111 aircraft and confirmed the performance increase: 20-30% range enhancement, 20% aerodynamic efficiency growth, and 15% increase of wing airload at a constant bending moment [6][7].

Szodruch and Hilbig [8][9] presented a variable camber wing concept to reduce drag and hence fuel consumption of a transport aircraft, with different wind tunnel results on wings of different cambers, wing design philosophy, systems requirements, and finally the benefits of new wing concept. A very relevant contribution on the design LE morphing concepts is due to Monner [10][11] within the ADIF project carried out by EADS-Airbus, DaimlerChrysler F&T and DLR, developed a concept to replace rigid, fixed ribs with a flexible alternative with a high stiffness (intended for large transport aircraft). The flexible plates were realized by combining several plates, contoured to the airfoil section shape, with revolute joints. The skin is allowed to move relative to the joint by incorporating slide joints and stringers to maintain stiffness. A proof of concept achieved the desired degree of camber. The research concentrated on the optimization of the rib elements to achieve minimum joint stress and maintain the camber objectives. After that, Monner focused on leading edge morphing, based on a collaboration between DLR and EADS

[1] Assistant Professor, Department of Aerospace Science and Technology, via La Masa 34, 20156 Milano, Italy, AIAA Member
[2] Research Assistant, Department of Aerospace Science and Technology, via La Masa 34, 20156 Milano, Italy
[3] Associate Professor, Department of Aerospace Science and Technology, via La Masa 34, 20156 Milano, Italy, AIAA Senior Member
[4] Associate Professor, Department of Aerospace Science and Technology, via La Masa 34, 20156 Milano, Italy
[5] Research Egineer, Aerodynamics Aeroelasticity and Acoustcis Department, 8 rue des vertugadins, 92190 Meudon, France, AIAA Member

within the SmartLED project. A smart leading-edge device was developed, which delivered an alternative to the droop nose device used by the A380: it was developed from Dornier Patent DE 2907912 using a suitable optimization process. The main emphasis of this new device was to realize a structure/system solution for a smooth leading surface, which can be deflected in a typical high-lift application: a deflection of 20deg was selected as the target. Starting from the work of Monner, different EU projects [12] where recently completed, such as SADE and SARISTU where a full scale wing section, characterized by a flexible, compliant skin actuated by a ad-hoc designed kinematics allowed to obtained smoothed and significant LE camber variations whose performances have been validated by wind tunnel tests. A similar solution for LE morphing, once again based on a flexible skin coupled to a rigid mechanism, was recently proposed inside the CS1-GRA platform proposed by Fraunhofer institute.

One of the major player nowadays in the field of wing morphing devices is represented by Flexsys Inc. [13][14] mainly focused on the aerodynamic smoothness of the wing and where they proposed a functional, seamless, hinge-free wing whose trailing and/or leading edges morphed on demand to adapt to different flight conditions. Kota presented results on a variable-camber trailing edge for a high-altitude, long-endurance aircraft, validated by a dedicated flight testing campaign. The airfoil flap system was optimized to maximize the laminar boundary layer extent over a broad lift coefficient range for endurance aircraft applications. The expanded 'laminar bucket' capability allows the endurance aircraft to significantly extend its range (15% or more) by continuously optimizing the wing L/D throughout the mission. The same technology was installed on the NASA Gulfstream aircraft by replacing the original flap with a new one embedding the same technology. A successfully flight test campaign was concluded recently. The key characteristic of the Flexsys approach is based on the use a fully compliant structure, without rigid mechanism.

Starting from the past studies available in the literature, and from ones directly acquired during the participation into recent EU projects such as SARISTU and NOVEMOR, the work carried out inside CS2-AG2 consortium aims at the introduction of a fully compliant structure for the LE morphing device so to guarantee the high lift requirements, especially critical in presence of a natural laminar wing such as one designed for the reference 90 pax twin prop regional aircraft.

II. Initial design requirements and adopted approach

The main goals of the morphing LE developed by AG2 consortium are based on the initial requirements synthesized in the following tables:

CONCEPT	SYSTEM FUNCTION	VALIDATION/DEMONSTRATION
Droop Nose	Seamless morphing leading edge section to improve high lift, low speed, Natural Laminar Flow wing aerodynamic performances of reference configuration	Large scale WTT aero-mechanical demonstration of advances HLD

Table 1. LE concept requirements.

SYSTEM	STRUCTURES	SUB SYSTEMS	ACTUATION TYPE
Doop Nose	Compliant ribs Compliant skin	Anti icing system Shape control Actuation	Electro Mechanical

Table 2. LE system requirements.

Together with the previous ones, specific performance requirements have been applied, in terms of CL max enhancement with respect the reference configuration, equal to 2.4% and 1.7%, considering both trailing and leading edge morphing effects in Take off and Landing, respectively.

Starting from these general requirements, a design procedure has been established based on five main steps:

1. Generation of the optimal aerodynamic shape to match the aerodynamic requirements at 2D wing section level;
2. 3D aerodynamic verification;
3. Generation of a possible skin configuration able to match the curvature requirements;
4. Optimization of the internal compliant structure able to guarantee, once actuated, to match the target aerodynamic shape, at 2D level;

5. Generation of the 3D configuration of the complete leading edge and 3D verification.

During the completion of the previously reported steps, both 2D as well 3D numerical models have been adopted with the fidelity level requested by the particular goal of each step. The following sections describe the activities carried out in the different steps.

III. Aerodynamic shape optimization and verification of morphing Leading Edge

The procedure, adopted in this work for the definition of the optimal morphing leading edge shape, consists of a shape optimization coupled with a parametric framework, able to design the optimal morphing shapes from the aerodynamic point of view, under skin structural requirements. The approach is able to combine the set of the most important cross–sections describing the wing, in order to define the optimal shape of a 3D morphing wing.

After the cross–sections are combined by PHORMA, a dedicated numerical tool described in [15], the 3D model of the wing is analytically defined so that its shape can be easily modified and used to estimate the aerodynamic performances. Different performance indices can be enclosed in the shape optimization process in order to improve the aerodynamic efficiency and to reduce the fuel consumption. A dedicated development of Class Shape Transformation (CST) method, extended by PoliMi to morphing wing sections [16], guarantees that the process works only on feasible shapes able to satisfy wing–box volume constraints and morphing skin structural requirements [15].

This parametric geometry representation is strictly related to an Object–Oriented Programming–based code that incorporates the ability to predict the structural response of the skin to the shape changes, provides couplings with aerodynamic solvers and integrates a CAD interface. From the aerodynamic point of view, a specific code is directly connected to the CST method for the automatic generation of structured meshes suitable to perform the high–fidelity 2D aerodynamic analyses of the most important cross–section of the aircraft. This last capability has been used during the shape optimization described in the next section.

A. Shape Optimization

The approach here adopted is based on a 2D shape optimization to match the CL max requirements, taking into account of the constraints on the structural properties of the skin. A dedicated optimization procedure, coupled with the parametric framework described in the previous sections, has been applied to the reference Regional Aircraft. The starting point has not been the Reference Wing, but directly the Loop1 optimized Wing, shown in Figure 1, coming from the contribution of ONERA inside the WP2.1.5, regarding the Natural Laminar Flow (NLF) wing. The process has already been applied to the shape optimization of morphing devices installed on regional and medium-size civil aircraft, as described in [17]. Here, the shape optimization was adopted in order to define the optimal morphing leading edge shape to be used as high-lift morphing devices.

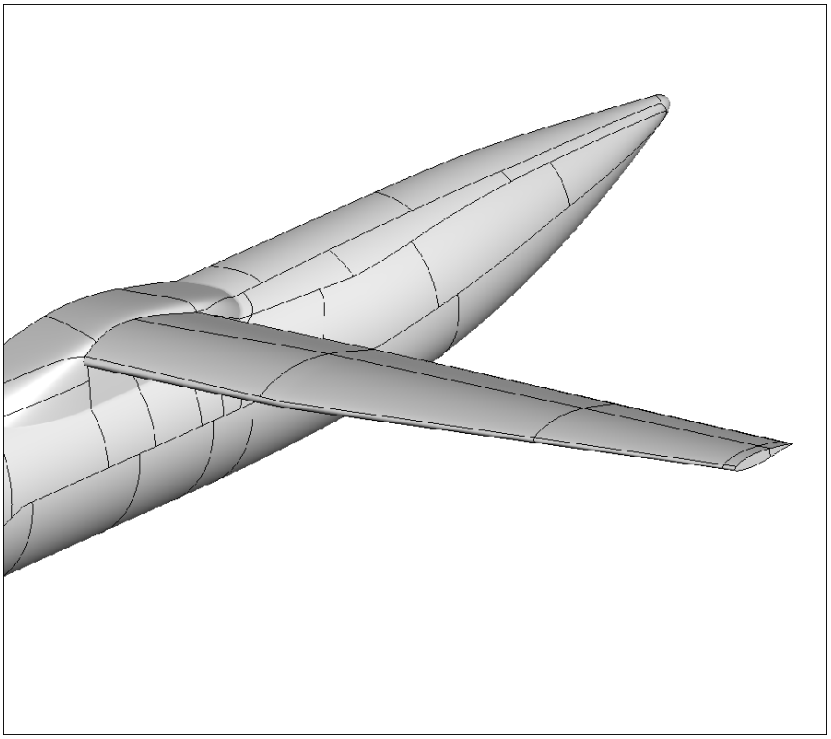

Figure 1. NLF optimized wing

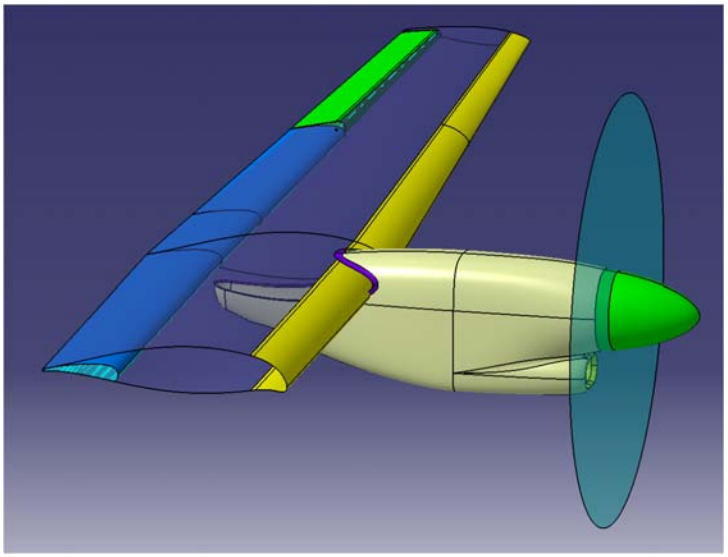

Figure 2. Reference Aircraft with morphing leading edge

The shape optimization process was run using an objective function that tries to introduce the maximum droop deflection along the wing span and, at the same time, reduce the drag coefficient Cd. This may be suitable for a single low–speed condition, corresponding to the landing condition of the Regional Aircraft here considered and to an angle of attack of 10 deg. A set of 4 parametric sections were identified along the span, but only the first three were used in order to introduce the morphing shape changes from the wing root to the first section of the aileron. The constraints introduced during the optimization include a linear deflection law in spanwise direction along the outboard region, while the maximum skin curvature change is set to avoid strains above 1.% , according to the Initial Design Requirements. Due to the high deflection levels, the curvature constraint is expressed in terms of curvature variation, that depends only on geometrical considerations, instead of bending stress, that depends on the material properties and

the skin thickness, unknown at this stage. The optimal shapes are chosen according to the following consideration: the alleviation of the bending stress inside the skin corresponds to the increase of the leading edge radius that helps to preserve laminar flow for low speed and high lift conditions. Figure 2 shows one of the optimal shapes obtained.
Four different morphing leading edge shapes were obtained by the shape optimization, the number 3 is shown in Figure 3 (left) as example. The spanwise droop deflection laws corresponding to the different shapes are very similar, the differences are mainly related to the leading edge radius and to the curvature distribution along the arc-length. For this reason, only a representative droop deflection law is shown in Figure 3 (right). The maximum droop deflection of section number 3 linearly decreases from δ_{LE}= 16.2° in the inboard region to δ_{LE}= 10.2° at the first section of the aileron, placed at 10.8m in spanwise. Between this section and the wing tip, the deflection gradually vanishes.

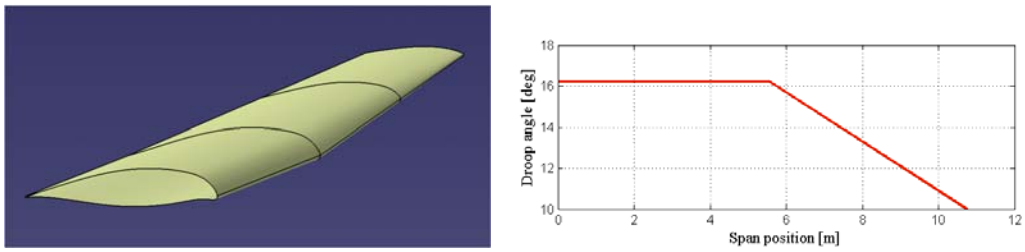

Figure 3. Optimal shape n.3 of morphing Leading Edge (left) and the related spanwise droop deflection law (right).

The 4 different morphing leading edge shapes obtained were analyzed from the aerodynamic point of view, considering the wing in landing configuration. In this phase, the effect of the droop nose has to be combined with one of the conventional trailing edge flap, which position is due to a rotation combined with translation movement and it is set to around 30 deg, while the corresponding landing flight condition around Mach = 0.2 SL. The aerodynamic analyses were performed by the MSES solver, which is a fully-coupled, implicit code, based on integral boundary layer (IBL) interaction [18]. Figure 4 shows the mesh of the corresponfing model. Different aerodynamic results were compared for both the inner wing region and for a section placed in the middle of the outer wing region, between the kink and the aileron. The use of the morphing Droop Nose improves significantly the maximum lift and the stall angle compared to the “clean nose” case and decreases the drag component, as shown in Figure 5.

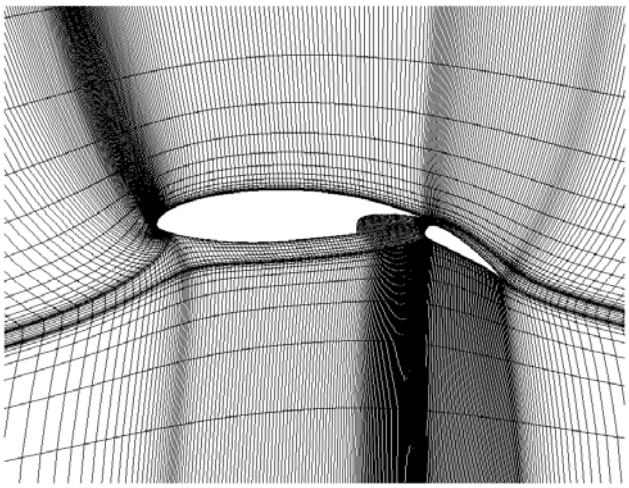

Figure 4. Aerodynamic model of the wing in landing configuration.

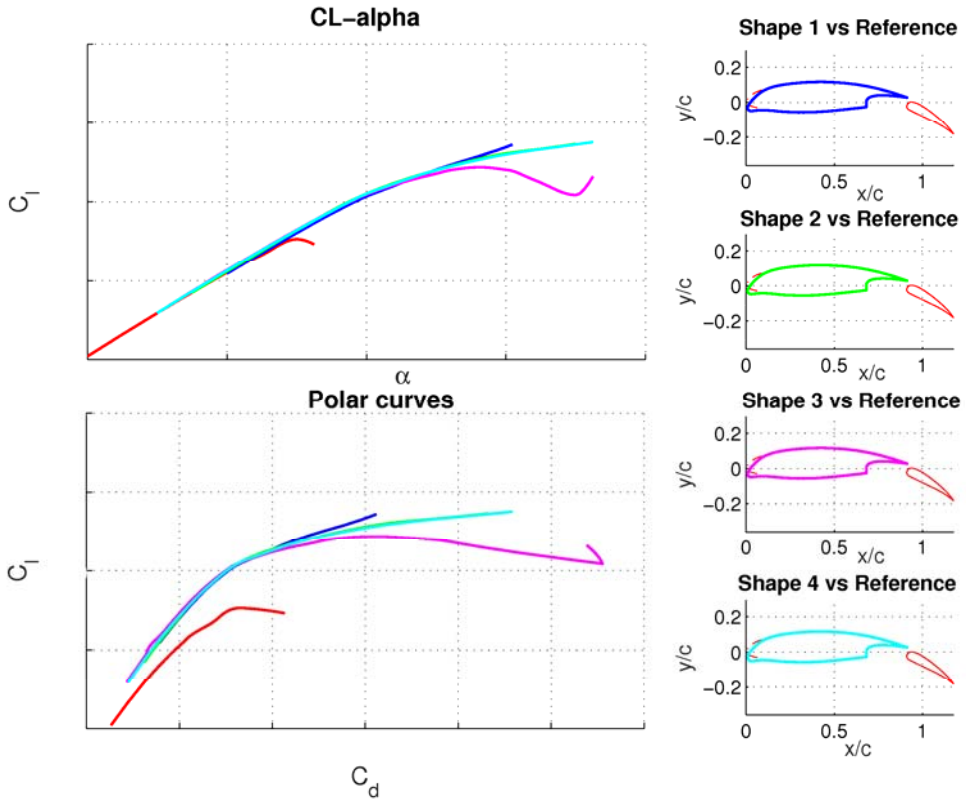

Figure 5. Comparison between the results of the aerodynamic analyses performed on the optimal morphing shapes obtained on the Outboard section.

B. Aerodynamic Validation

Additional aerodynamic analyses were performed in order to validate the 2D results obtained along the span and to select the best morphing leading edeg shape.

A final performance assessment using 2D RANS simulations with the Onera elsA software [19] determined the choice of two best candidates for morphing leading edge shape to be adopted for the final 3D simulations, represented in Figure 6. At a given angle of attack, the effect of the morphed leading-edge leads to a strong decrease in the maximum velocity peak at leading-edge, that delays significantly the stall onset on this wing section (Figure 7).

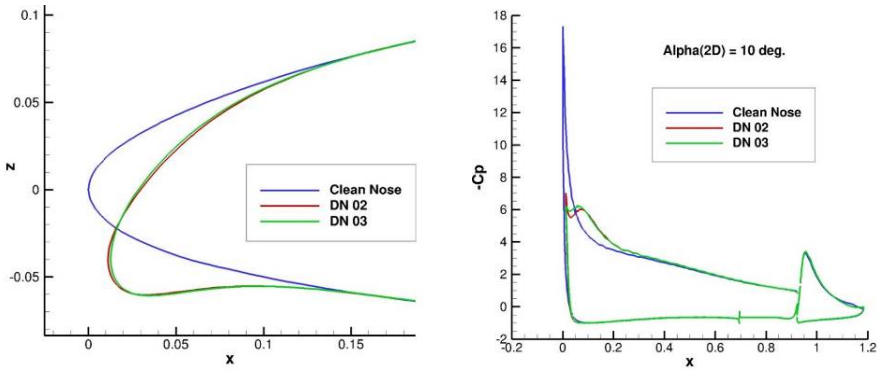

Figure 6. 2D aerodynamic results in terms of Cp distribution in Landing condition, at constant alpha.

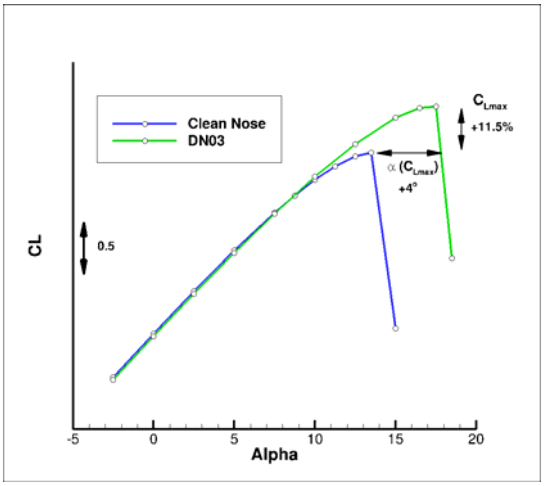

Figure 7. 2D $C_L(\alpha)$ curves

C. Aerodynamic assessment of the morphing device efficiency on aircraft

Finally, the assessment of the aerodynamic efficiency of the morphing device on 3D aircraft configuration at low speed has been carried out on the NLF wing designed in AG2 project, derived from the reference 90 pax turboprop regional aircraft. A new flap system has been designed and adapted to this NLF plane and the morphed leading-edge shape obtained previously has been adapted to the new wing shape. Both aircraft consider similar wing planform and the airfoil shapes at the leading-edge region are quite similar, even though obtained by different optimization processes. Therefore, the adapation of the morphed leading-edge shape to the NLF wing was not too difficult.

Three dimensional RANS computations have been carried out using the Onera elsA software [19] in fully turbulent mode. As these computations took place within a more global design process, the chimera overset grid technique has been applied for the flap element, with the Onera Cassiopee suite [20] used for pre-processing. Figure 8 presents the configurations considered. They are considering :

- The fuselage, the belly fairing and the karman ;
- The NLF wing equipped with a reference winglet, with the flap cove :
  - with a clean leading-edge, or ;
  - with the 3D morphing leading-edge
- A 3D flap at optimized take-off settings (Flap deflection : 20°).

Note that the nacelle is not taken into account.

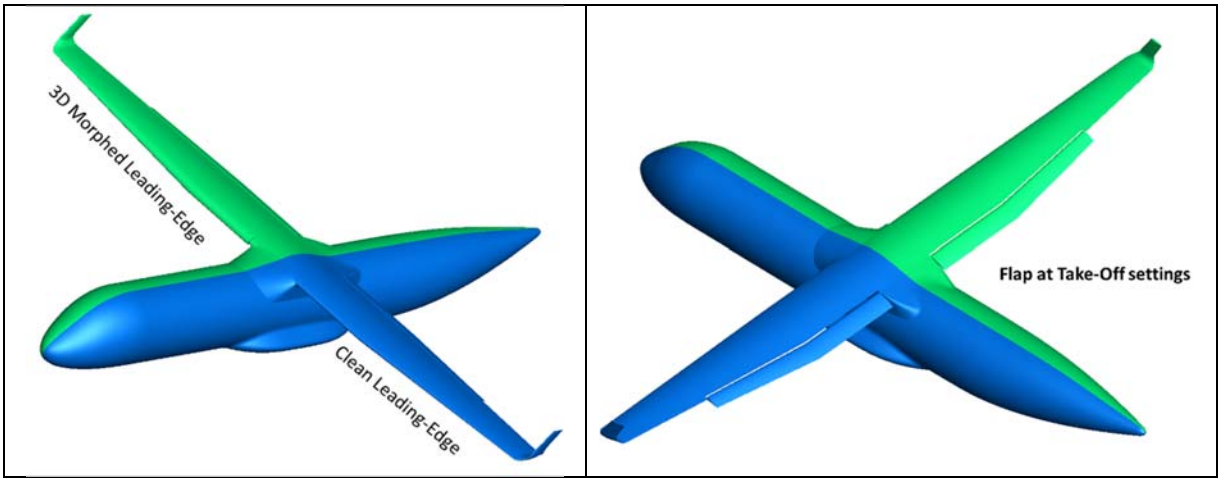

Figure 8 – Aircraft configurations considered for the 3D aerodynamic performance assessment.

Figure 9 presents the computed $C_L(\alpha)$ curves for configurations with or without morphed leading-edge at take-off conditions (M=0.197 at sea level). As for the 2D evaluation, there is a significant delay of stall onset observed on the 3D performance by the use of the morphed leading-edge device. Figure 10 compares the pressure field on the wing at high angle of attack (α=12.5°). It can clearly be seen that the use of the morphed leading edge decreases significantly the maximum local velocity peak at the wing leading edge. Therefore, the leading-edge stall onset is delayed.

The gain in stall angle (+2.5°) is lower than the one obtained in 2D (+4°), because the wing section selected for 2D evaluation is not the one that stalls on the wing, located on the outer wing. In addition, there is a spanwise variation of the deflection of the morphed leading edge, which has lower value at wing tip than at wing root. However, the gain in maximum lift coefficient is significant (+10%).

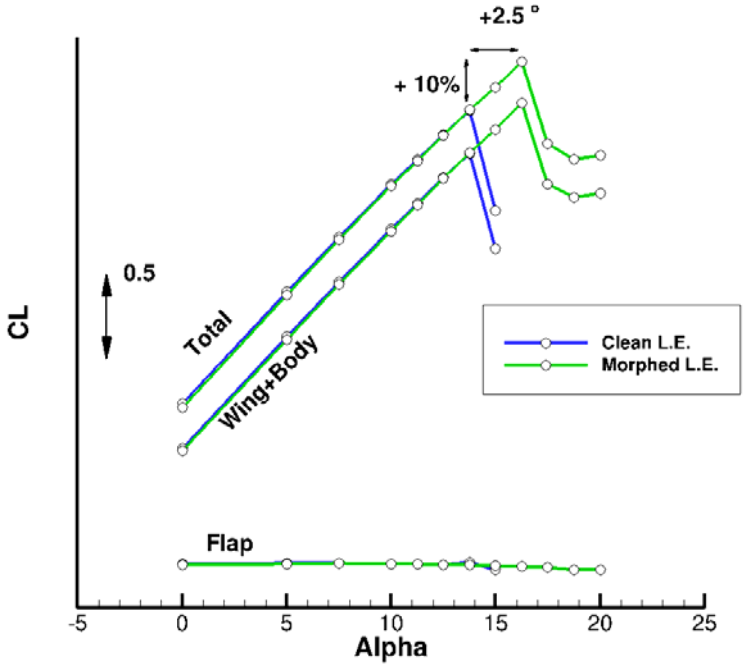

Figure 9 : Computed effect of 3D morphed leading-edge on $C_L(\alpha)$ curves – Take-Off configuration.

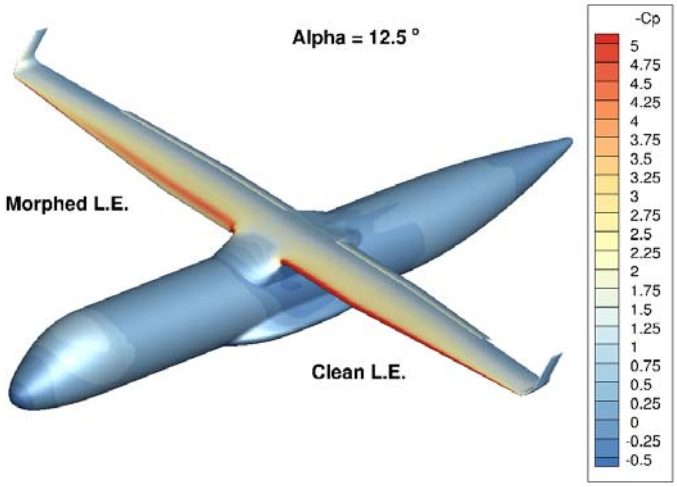

Figure 10: Effect of morphed leading-edge on pressure distribution – Take-Off configuration, incidence=12.5°.

In term of aerodynamic efficiency, the use of the morphed leading-edge applied to the NLF wing defined within the AG2 project leads to significant gain in maximum lift performance of this TP configuration. Meeting the aero requirements at low speed while maintaining a laminar flow extent at cruise for the NLF wing seems possible only by the use of such device.

IV. Design of the morphing skin

The structural design of the morphing skin is composed by two main activities. The definition of the optimal actuation points which represent the best arc-length positions where the morphing mechanism can be connected in order to introduce the shape change in the most efficient way. Then, the study of the structural configuration of the morphing skin, before the internal mechanism is defined, using the same points to introduce the enforced displacements corresponding to the shape changes, defined in the previous section.

A. Definition of the optimal active actuation points

The parametric methods, embedded into the CST representation, are used to determine the active point locations which are provided in output as non–dimensional arc–length along the skin [16]. Together with the definition of the optimal morphing shape, the optimal actuation points allow to perform preliminary studies on the morphing skin configuration, before the internal mechanism is defined.

After the optimal morphing shape is defined, the optimal locations of a fixed number of actuation points can be found. They are defined as the best non–dimensional arc–length positions along the skin of the points where the morphing mechanism can be connected to introduce the shape change in the most efficient way.

The compliant mechanism can transmit the input actuation motion through these active points to control the motion/shape of the morphing skin. The active points also represent the 'output points' of the internal compliant mechanism which are included between the Genetic variables described in Section V. A compliant mechanism connected to every point along the skin might excessively increase the number of design variables. For this reason, a fixed number of required active points which allows the compliant mechanism to achieve the target shape change with acceptable error, must be identified.

Figure 11: Skin actuation point optimization scheme

This problem is implemented as an optimization algorithm, shown in Figure 11, where a piecewise linear interpolation function is used to fit the curvature difference function $\Delta\kappa(nal)$, defined in [16] and computed between the undeformed shape and the optimal morphing shape obtained during the shape optimization. The designer fixes the number of active points and a continuous optimization process, coupled with the CST method, is used to find the optimal locations of the active points as the ends of each piece (of the piecewise linear interpolation), while the optimization constraints avoid the active points overlap each other and they go out of design domain. A Sequential Quadratic Programming (SQP) method is employed and the objective function is defined as the fitting error between the curvature difference function interpolated and computed by the CST method. Figure 12 shows the location of the output active points for a morphing leading edge.

After the unfeasible or inaccessible active points have been discarded and when the output active point number and locations are defined, the designer can specify the minimum discretization mesh size of the skin model, in order to improve the resolution of the results. The additional points introduced along the boundary allow to spread out the pressure load, coming out from the aerodynamic analysis, on the airfoil skins.

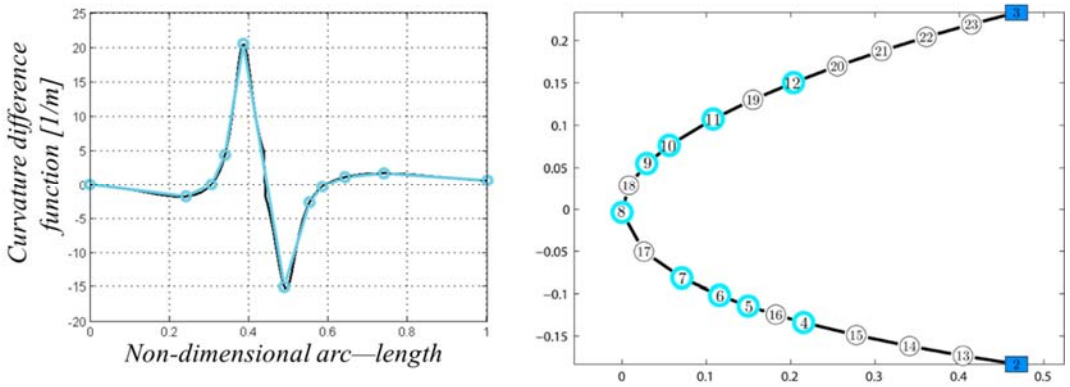

Figure 12. Optimal active point locations which better allow to fit the curvature difference function between the undeformed and the morphing leading edge, computed by means of the semi-analytical CST arc length method.

B. Skin Structural Definition

The aim of this step is a comparative study on different structural skin configurations. Two-dimensional and three-dimensional behaviour evaluations, in terms of shape quality and maximum strains comparisons, under pressure distribution along LE skin, were performed on the configurations reported in Figure 13.

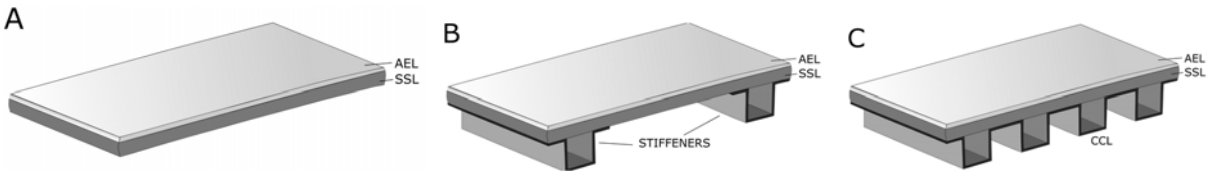

Figure 13. Different skin structural configurations.

Three different configurations were examined, i.e.:

A. NRSC - Not reinforced skin;
B. SRSC - Simply-reinforced skin;
C. CCSC - Corrugated skin.

For all the considered structural configurations, the skin is assumed as composed of two layers:

1. AEL (ANTI-EROSION LAYER) material: Titanium, thickness: 0.10mm
2. SSL (SKIN STRUCTURAL LAYER) material: FRP (Fiber reinforced polymer) composite

Finally, two SSL laminations are examined:

- Total Glass fibers: reinforced polymer (GFRP) Fabric
- Hybrid lamination: half-thickness GFRP Fabric + half-thickness Carbon fibers reinforced polymer (CFRP)

The hybrid configuration is selected for SSL lamination of Not-reinforced skin solution. Hybrid lamination provides higher bending stiffness for the same total thickness and the addition of CFRP under AEL generally exhibits a strain reduction into AEL.

In case of simply reinforced skin, stiffeners are used in order to reinforce the skin and to introduce the physical connections between the skin and the morphing ribs, in the actuation points defined in previous Subsection. The SSL/AEL laminations are equal to the Not-Reinforced Skin. The lamination sequence of the stiffener is a symmetrical lamination (GFRP with CFRP core) with thickness equal to local SSL thickness. The LE skin is divided in four constant properties (thickness) sections and two different stiffeners geometries, for low and high curvature areas, are used along each section, as shown in Figure 14.

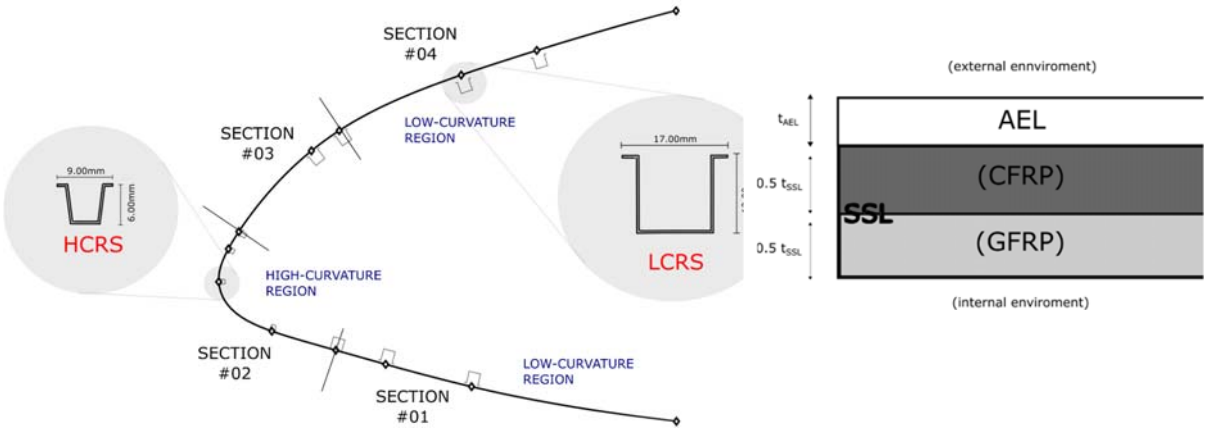

Figure 14. Lamination sequence of the Simply-Reinforced configuration along the leading edge skin.

Finally, in the corrugated skin, the SSL/AEL laminations is equal to the not-reinforced skin along the 4 regions, while the Composite Corrugated Layer (CCL) shows a symmetrical lamination sequence composed by GFRP lamination with CFRP core and thickness equal to half local SSL thickness. In the high curvature region (Section #02) the CCL is not added, while it is used for all other three sections, as shown in Figure 15.

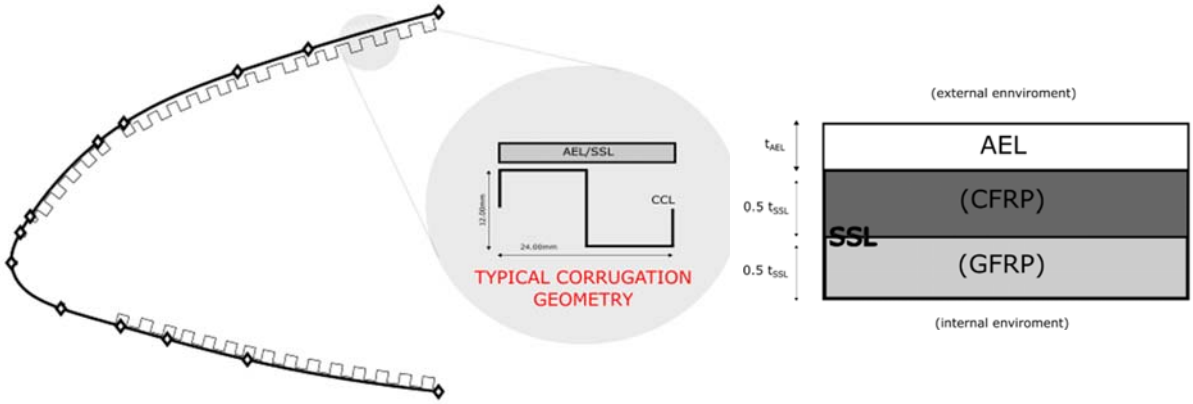

Figure 15. Lamination sequence of the Corrugated leading edge skin.

The skin design in terms of thickness distribution, as in the case of the actuation point locations, depends on the design of the internal mechanism which has to introduce the shape modification. At this stage only the optimization of the thickness distribution is performed, in order to define the most suitable material properties and the range where the thickness can change. The skin structural solution was found by an optimization process where the objective function is represented by the maximization of the skin bending stiffness chordwise and the constraints are the same used in the aerodynamic shape optimization: the maximum skin curvature change, adopted in the shape optimization, is reported here as a maximum strain of 0.010. The optimization variables are the thickness of the four sections shown in Figure 14. Considering the SSL hybrid lamination with a fixed ratio between the thicknesses of the CFRP and GFRP layers equal to 1.00 and the typical stringers and CCL geometries (Figure 14 and Figure 15), the optimal thicknesses distribution of the external skin has been obtained.

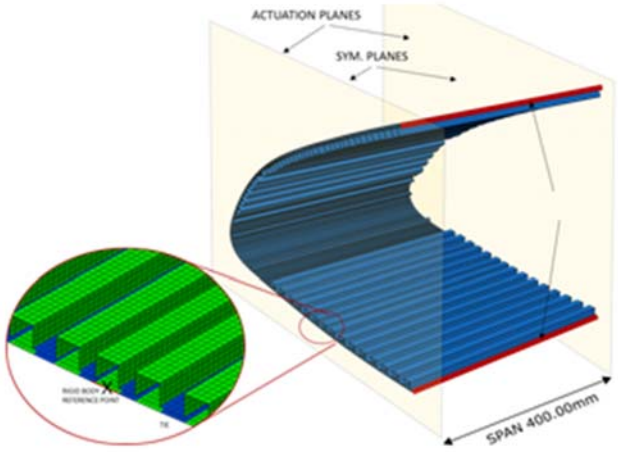

Figure 16 - Structural model of the leading edge skin between two adaptive ribs.

The optimization is based on 2D and 3D static implicit non-linear multi-step analyses performed by the Abaqus Standard-Implicit code. In the case of 2D analysis, one row of elements in span-direction and out-of-plane symmetry constraints are used. In the 3D analyses, the actuation and the symmetry constraints planes shown in Figure 16, are used to simulate the behaviour of the skin region between two adaptive ribs spaced 400mm. The actuation steps act on the optimal active points, computed in Subsection IV.A. Pressure loads, coming from the aerodynamic analyses performed on the same morphing shape, are applied along the skin by surface distribution, constant on single element.

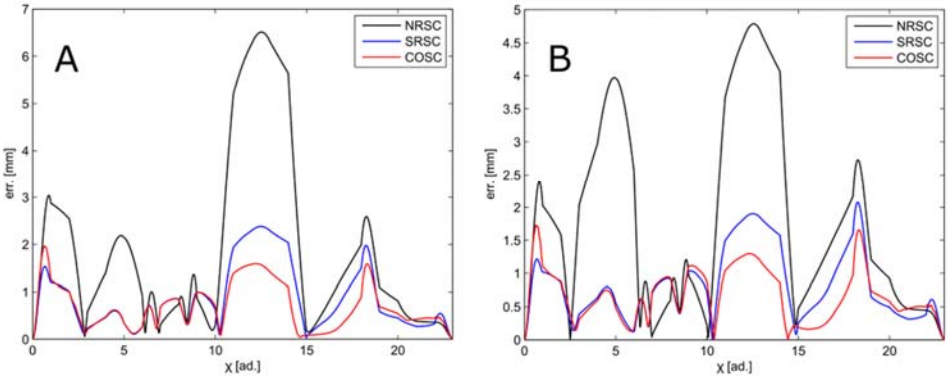

Figure 17 – Shape error under actuation laods (A) and both actuation/pressure loads (B) in the middle-span location

Figure 17 shows the shape errors evaluated with comparison to the target curve in the cross-section placed in the middle-span location of the aforementioned 3D model. The errors are reported vs. the non-dimensional 2D arc-length for the three analyzed configurations. The not reinforced solution exhibits an unsuitable 3D shape quality under actuation loads and does not provide enough bending stiffness in span direction. Reinforced solutions minimize the anticlastic deformations with a percentage reduction of the shape mean square error in the 76% - 82% range with comparison to the not reinforced configuration. Similar performances in terms of out-of-plane bending stiffness for both reinforced solutions (Simply and Corrugated) were obtained, but the use of Corrugated in high-curvature regions does not provide significant benefits. The corrugated skin does not provide significant advantages, in terms of shape error under pressure loads, with respect to the simply reinforced skin. Moreover the corrugated solution presents some disadvantages:

- Does not provide advantages in bending stiffness for the same maximum strain and curvature. It generally presents higher strains.

- The LE skin is characterized by small section lengths, so the Corrugated presents a cell miniaturization problems related to the technological process adopted.

For all these reasons, the proposed solution to be used for the design if the internal is represented by the AEL/SSL hybrid lamination in the simply-reinforced skin configuration, leaving the use of Corrugated skin in case the optimal configuration of internal compliant mechanisms produces very large un supported panels.

V. Preliminary design of the compliant LE structure

The design of compliant mechanisms for the leading edge is performed using a code dedicated to the morphing aircraft design named SPHERA (Synthesis of compliant mecHanisms for Engineering Applications). The proposed approach is based on a multi-objective optimization coupled with a Load Path Representation and Genetic Algorithm [16].

Compliant mechanisms designed by SPHERA are able to meet both kinematic (motion) and structural (load-carrying) requirements, considering the mechanism design and the structure design, respectively, for a number of load conditions corresponding to the analyzed aerodynamic conditions. This is a typical multi-objective design problem that can be efficiently incorporated into a genetic algorithm [21]. The approach used for solving this kind of problems applied to our purposes is the so called Elitist Non-Dominated Sorting Genetic Algorithm (NSGA-II) [22].

Different kinds of objective function can be considered. The first one is the minimization of the error, in a least square sense, between the deformation of the compliant mechanism once actuated and the optimal target shapes obtained by the shape optimization of Section III.A (kinematic requirement). The comparison between the two shapes is done for a discrete number of control points distributed over the airfoil skin. The second one represents the minimization of the Strain Energy (structural requirement) when the morphing mechanism is loaded by the external aerodynamic loads, while the actuation input point is kept fixed. Each objective function can be associated with a user-defined number of design load conditions, increasing the total number of objective functions. An optional objective function is related to the minimization of the stress inside the mechanisms.

The multi-objective Genetic Algorithm find multiple optimal solutions represented by a Pareto Front. At the end of the process, the designer selects the design point directly from the Pareto Front, taking into account manufacturing requirements, not included in the optimization problem. In the case here described, in order to simplify the optimization problem and to limit the potential size of the design space, the multi-objective optimization problem is formulated as a 2D problem, finding the optimal compliant structure for a selected rib, later extended to the complete 3D space.

A. Multi-objective Optimization

The structural definition of the LE compliant ribs was carried out by a specific code, starting from the morphing target shape, obtained by previously described shape optimization and characterized by 16deg droop angle. This code is based on a multi-objective genetic algorithm and a combination of multiple objective functions was considered. Different flight conditions, corresponding to the MCC, should be used both in the structural and the kinematic requirements. However, this preliminary design is performed considering only three main objective functions:
The load path representation method is coupled with a nonlinear analysis solver, based on Finite Volume Beam elements [23]. The Finite Volume C0 Beam is a three-node non-linear beam based on a collocated evaluation of internal forces and moments.

Once the skin structural configuration has been defined, the thickness distribution along the skin is still introduced, as design variable, in the optimization of the compliant device because it depends also on the type of mechanism. The results of the skin structural optimization, were used to compute the equivalent Young's modulus/skin thickness variation law, based on the previous structural skin configuration to be used during the compliant structure optimization.

The structural definition of the LE compliant ribs was carried out by means of a dedicated design code, starting from the morphing target shape, obtained by the shape optimization and characterized by *16 degs* droop angle. For a proper execution of the multi-objective genetic algorithm, the combination of the following objective functions has been considered. Different flight and mass conditions should be used both in the structural and the kinematic requirements. However, this preliminary design is performed considering only three main objective functions:

1. **Structural requirement**: minimizing the Strain Energy (SE) to preserve NLF wing shape. Morphing mechanism kept fixed under the aerodynamic loads, at Mach = 0.48 (Sea Level, Dive Speed), corresponding to the Dive Speed and shown in the left side of Figure 18→ *Linear Analyses*;;

2. **Kinematic requirement**: minimizing the Least Square Error (LSE) between Target and Deformed LE shape, when the mechanism is deployed, under the external aerodynamic, at Mach = 0.197 (SL and alpha = 10deg, Landing flight condition), corresponding to the landing flight condition and shown in the right side of Figure 18→ Nonlinear Analyses;

3. **Minimizing the maximum:** Minimizing the maximum value of internal stress, when the mechanism is deployed, under the same external aerodynamic loads considered in the 2nd objective function.

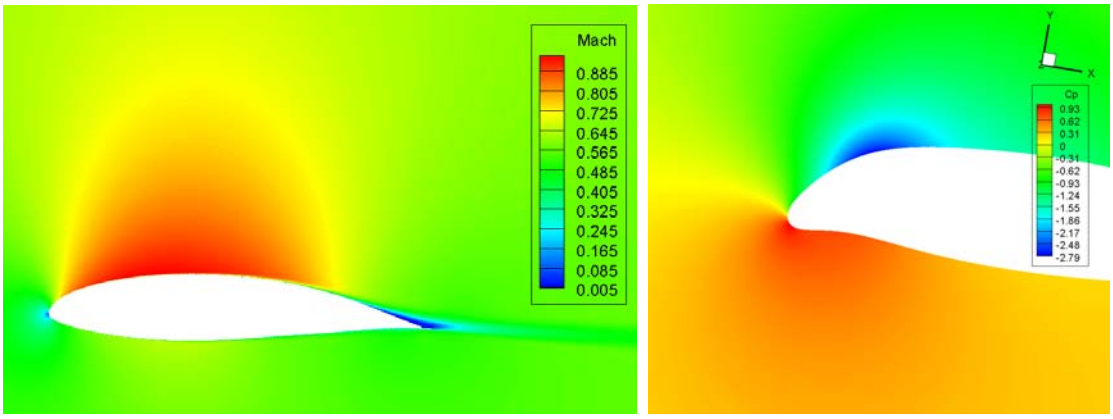

Figure 18. Aerodynamic loads corresponding to the structural (left) and kinematic (right) requirements.

The leading edge target shape change was obtained by imposing a skin constant length. In this way the morphing LE can change its aerodynamic shape in an efficient way, without generating axial stresses inaide the skin. The corresponding leading edge structural model was characterized by two clamps at the upper and lower skin connections with the structural interface points (2 and 3 in Figure 19), while an horizontal actuation force is pushing in the left direction trying to deflect the leading edge downward (point 1). A total of 9 active output points (4 to 12), defined in Section IV, was used for transferring the actuation loads from the inner compliant mechanism to the outer skin. Additional deactivated points were also introduced along the leading edge contour in order to improve the resolution of the results and to better distribute the aerodynamic loads. Figure 19 on the right shows one set of external loads coming from the aerodynamic computations and transferred to the structural grid points. A total of 10 separate regions along the leading edge boundary, where thicknesses vary interdependently in the course of the optimization process, were used. Moreover 5 internal points (24 to 28), were collocated in the user-defined airfoil domain to automatically define the initial population of load paths.

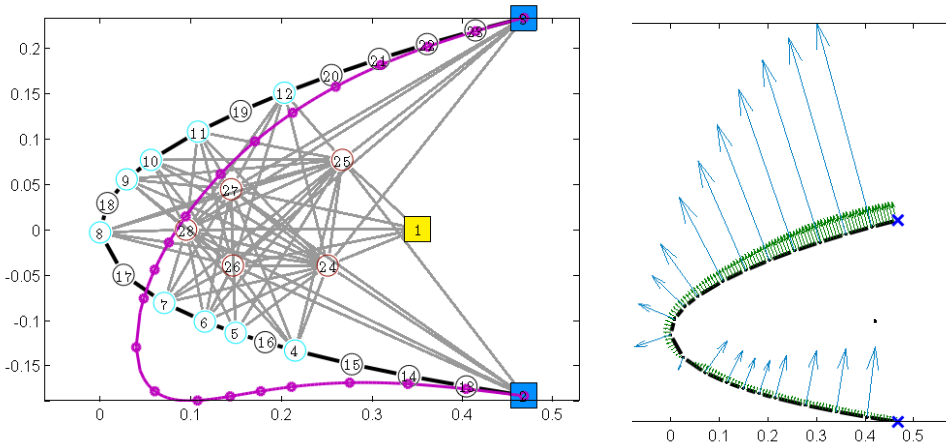

Figure 19– Initial population and aerodynamic load application corresponding to the kinematic requirements.

In this design case, the stress constraint, considered during the shape optimization described in Section III as maximum curvature difference, does not include the skin. The genetic algorithm accounted an initial population of 280 individuals and was left free to run for 600 generations. After 420 iterations a Pareto Front was invoked, which made easier to identify the best design trade-off between kinematics, structural and stress objectives in terms of LSE deviations. Figure 20 and Figure 21 show Pareto front solutions obtained for the previously introduced leading edge and the selected design point. In particular the point highlighted with red color represents the best compromise between the three objectives and shows a LSE value of 0.0113 m, concerning the kinematic requirement. During the optimization, the load path cross-sectional thickness was free to vary between *0.4mm* and *6mm*. The required deformation behaviour led to a total requested actuator stroke for the complete morphing equal to *3.6cm* with an angle of *10deg* downwards.

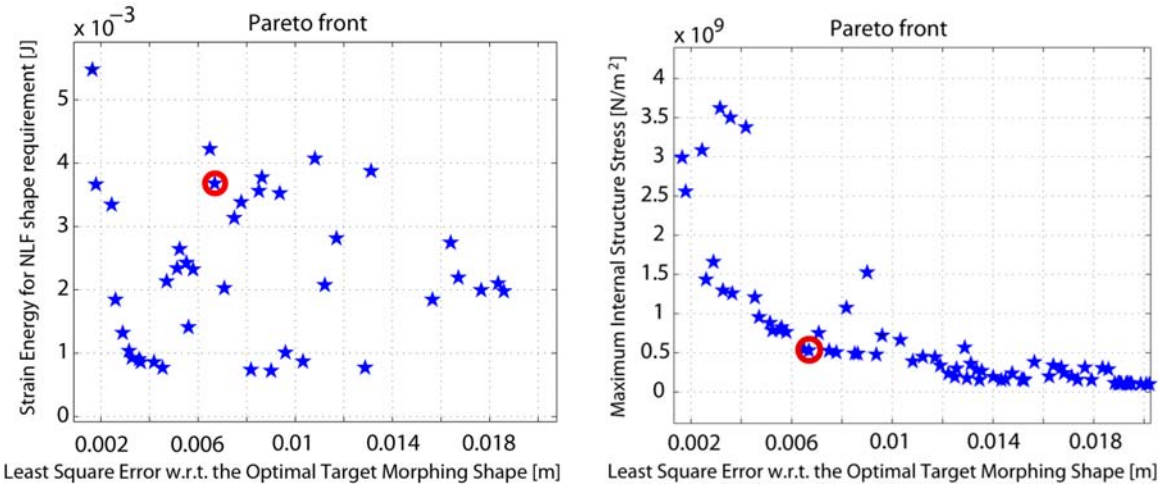

Figure 20. Typical Pareto fronts.

The solution selected on the Pareto front is refined by a gradient—based optimization (SQP) where the LSE is the single objective function, while the Strain Energy (SE), to preserve the NLF wing shape, and the maximum value of internal stresses become two non—linear constrains.
The variables are the same ones used during the Global Optimization based on GA, except for the topology variables: the number of load paths can not change.

Starting from the final 2D compliant solution, a specific interface between SPHERA and PHORMA allows to automatically generate corresponding 3D FEM models. Depending on the required analysis, different solvers can be invoked: hybrid models, composed by beam and plate elements, for MSC/Nastran software or more general ANSYS models can be produced [21][24]. In the case of this work the same scripts, already used during the morphing skin design and based on Abaqus-based non-linear analyses, are to generate the complete 3D FEM models.

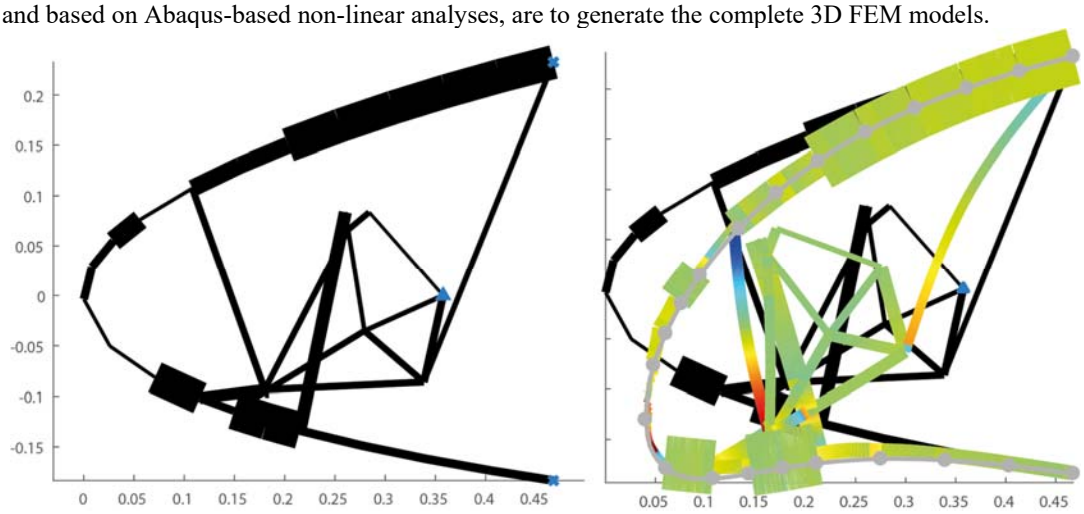

Figure 21. Comparison between two different optimal configuration of morphing mechanism.

B. Structural verification

Once the structural configuration of the skin and the internal compliant mechanism have been defined, a detailed 3D FEM model of the final design is carried out. An accurate modeling of the stringers and their connections with the adaptive ribs is introduced in order to evaluate the stress concentrations and their effects on the structural response. The objectives of the detailed model can be summarized as follows:

- improve the optimized solution in order to obtain a technological feasible configuration
- verify the structural integrity of the final configuration under the actuation and pressure loads
- evaluate the actuation loads required to obtain the final morphed shape

For such a reasons the skin is divided in additional sections in order to minimize the severe skin thickness discontinuities due to the few design variables used in the preliminary 2D structural optimization of Section IV.B (10 sections). Beside the technological issues, the smoother thickness distribution in the chord-direction is also used to reduce the strain localization into the skin.

Different structural solutions could be investigated in order to correctly distribute the deformation along the span in a more efficient way which try to save the total weight of the morphing device. If the solution based on *400mm* spaced ribs requires more thicker ribs and a reinforced skin layer composed by more stiffeners, a "bio-inspired" configuration based on a higher number of compliant ribs allows to reduce the thickness of the ribs and the number of stiffeners, only used as connection between the load paths and the skin. This second solution has been selected for the structural assessment.

The 3D analyses are based on the same solver used during the design of the morphing skin and described in Section IV.B. The static implicit non-linear multi-step analyses, performed by the Abaqus Standard-Implicit code, were set using the following parameters:

1. Equation solver: Standard Newton solver
2. Relative tolerance for convergence (RESIDUAL): 10^{-3}
3. Maximum number of iterations allowed: 300.
4. Maximum number of time increment: 100.

RESIDUAL: The error in the approximate solution is measured by the relative residual, defined by $\|Ku - f\|/\|f\|$, where $\|\cdot\|$ is the L^2 norm. $Ku = f$ is the corresponding linear system, where K, u and f are the stiffness matrix and the displacement and force vector, respectively. The input actuation is introduced through a rotation of 80 deg of a shaft connected to the compliant ribs by a rigid kinematic chain, shown in Figure 24 with yellow color. The aerodynamic loads are applied to the skin surface, as a Cp distribution corresponding to the Landing flight condition at Mach = 0.197 (SL) and alpha = 10deg.

The undeformed and deformed configurations of the final 3D model are given in Figure 22, while Figure 23 provides the strain distribution in the external titanium layer of the skin (AEL).

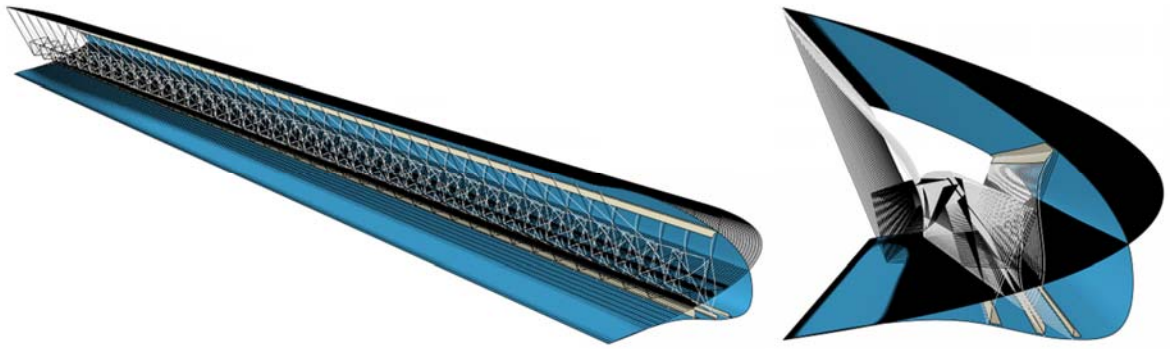

Figure 22. views of the final detailed model

As for the aforementioned model, the strains have a quite constant distribution in the span-direction. The maximum strain in the layer is 8988 mirostrain, close to the skin structural constraints imposed in the aerodynamic optimization (10000 microstrain). The difference could be also explained in terms of modelling techniques. The equivalent-stiffness

shells used in the optimization process are not able to describe the true position of the neutral plane of the skin. Indeed, one of the main advantages of the SSL hybrid lamination, that can be described only through a multi-layer shell model, is the minimization of the strain into the more critical external layer moving outwards the skin neutral plane. This phenomenon can be detected also in the case of pure bending condition that represents the situation forced in the optimization process.

The use of a titanium alloy for the manufacturing of the anti-erosion layer is not suggested for the considered level of deflection, because of the high load conditions that could cause severe fatigue troubles. The reducing of the deflection, in accordance with the aerodynamic performance increment, should be taken into account. Alternatively, different anti-erosion shields have to be investigated.

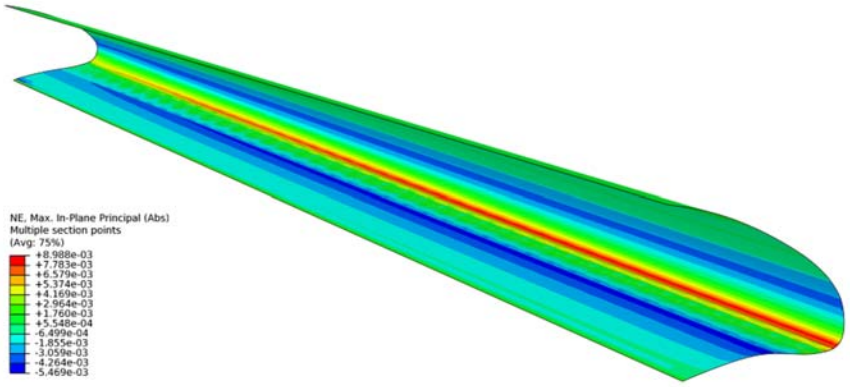

Figure 23. Strain distribution into the external anti-erosion layer (AEL).

This configuration shows how it is able to obtain an uniform stress distribution in span direction with a limited use of additional structural components, as stiffener of reinforced skin layer. Moreover the results obtained from these high-fidelity structural models represent an important verification that confirms how the stress constraint used during the shape optimization allows to simplify the problem definition for the optimization of the compliant device.

C. Morphing device installation and preliminary assessment

A solution where the distance between two adaptive ribs is equal to 260mm, and three stringers are used to connect the compliant ribs and the morphing skin, is shown in Figure 24. This solution has been investigated and the corresponding CAD model produced. This model, together with the high-fidelity non-linear FEM model presented in Section V.B, allowed to estimate some global index related to the weight and to the power consumption of the morphing leading edge device.

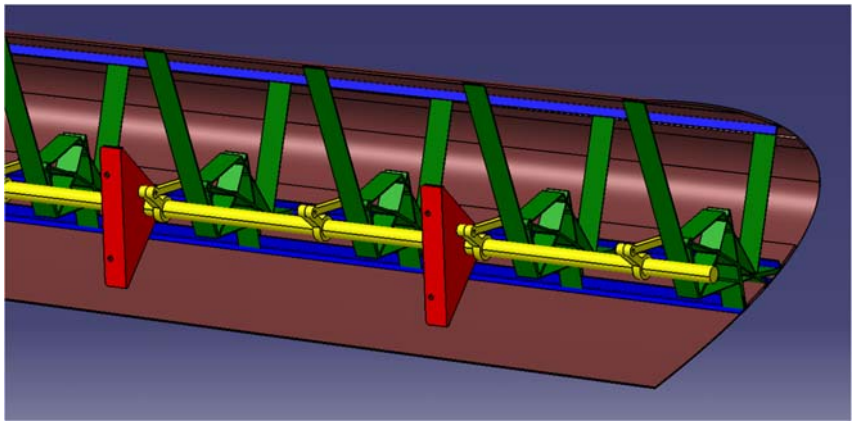

Figure 24. 3D actuated compliant leading edge.

The summary of preliminary results include:

- Weight due to the installation of the morphing Droop Nose, including morphing Skin and internal Compliant Structure (weight of the actuators is not included):
  Inboard region (before the nacelle): Total weight ≈ 11 kg/m
  Outboard region (after the nacelle): Total weight ≈ 9.2 kg/m
- Power consumption: The actuation rate from undeformed position to max. deflection is assumed ≤ 20 s (TBC), while the required torque is:
  Inboard region: 500 Nm
  Outboard region: 850 Nm

The results in terms of total weight can be compared with typical values for LE which on similar aircraft are 13 and 6.5 kg/m, with and without slat, respectively.

VI. Conclusion

The present work described the conceptual design of a morphing Leading Edge device to be applied to novel twin-prop regional aircraft. The conceptual design involved the definition of the optimal aerodynamic shape as well an investigation of possible configuration in terms of skin and internal structures. The structural investigations found a possible configuration for the skin (reinforced configuration) and for the internal structure (light compliant ribs in a high density configuration) actuated by a linear mechanism connected to a single rotating actuator. High-fidelity 3D aerodynamic validation confirmed the performances predicted at conceptual level using simplified 2D models, while the results coming from the preliminary structural design allowed a detailed estimation of the total weight and the power consumption required by the complete compliant leading edge device.

Acknowledgments

The research leading to these results has received funding from the European Community's Seventh Framework Programme (FP7/2007-2013) for the Clean Sky Joint Technology Initiative under grant agreement CSJU-GAM-GRA-2008-001 and the European Community's Horizon 2020 - the Framework Programme for Research and Innovation (2014-2020) for the Clean Sky Joint Technology Initiative under grant agreement CS2-REG-GAM-2014-2015-01.

References

[1] S. Barbarino, O. Bilgen, R.M. Ajaj, M .Friswell and D.J. Inman, A Review of Morphing Aircraft, Journal of Intelligent Materials and Structures, Volume: 22, issue: 9, 2011, page(s): 823-877. doi: 10.1177/1045389X11414084

[2] Boeing, Aerospace Company. ''Variable Camber Wing", Second Progress Report, AD911543. June 1973

[3] de Camp, R.W. and Hardy, R. 1984. ''Mission Adaptive Wing Advanced Research Concepts,'' AIAA 1984-2088, 11th Atmospheric Flight Mechanics Conference, Guidance, Navigation, and Control and Co-located Conferences, Seattle,WA,U.S.A., 21 August 1984 - 23 August 1984. doi: 10.2514/6.1984-2088

[4] Bonnema, K.L. and Smith, S.B. 1988. ''AFTI/F-111 Mission Adaptive Wing Flight Research Program,'' In: Proceedings of 4th AIAA Flight Test Conference, 18-20 May, San Diego, CA, pp. 155-161.

[5] Spillman, J. 1992. ''The Use of Variable Camber to Reduce Drag, Weight and Costs of Transport Aircraft,'' *Aeronautical Journal*, 96:1-9.

[6] Smith, J.W., Lock, W.P. and Payne, G.A. 1992. ''Variable Camber Systems Integration and Operational Performance of the AFTI/ F-111 Mission Adaptive Wing,'' Technical Memorandum, NASA Dryden Flight Research Center, Edwards, CA.

[7] Smith, S.B. and Nelson, D.W. 1990. ''Determination of the Aerodynamic Characteristics of the Mission Adaptive Wing,'' *Journal of Aircraft*, 27:950-958.

[8] Szodruch, J. 1985. ''The Influence of Camber Variation on the Aerodynamics of Civil Transport Aircraft,'' In: Proceedings of 23rd Aerospace Sciences Meeting, 14-17 January, Reno, NV, AIAA 85-0353.

[9] Szodruch, J. and Hilbig, R. 1988. ''Variable Wing Camber for Transport Aircraft,'' *Progress in Aerospace Sciences*, 25:297-328.

[10] Monner, H.P., Bein, T., Hanselka, H. and Breitbach, E. 1998. ‘‘Design Aspects of the Adaptive Wing ! The Elastic Trailing Edge and the Local Spoiler Bump,’’ Royal Aeronautical Society, Multidisciplinary Design and Optimization, London, UK.

[11] Monner, H.P., Kintscher, M., Lorkowski, T. and Storm, S. 2009. ‘‘Design of a Smart Droop Nose as Leading Edge High Lift System for Transportation Aircrafts,’’ In: Proceedings of 50th AIAA/ASME/ASCE/AHS/ASC Structures, Structural Dynamics, and Materials Conference, 4-5 May, Palm Springs, CA, AIAA 2009-2128 (10 pp).

[12] Lajux, V. and Fielding, J. 2005. ‘‘Development of a Variable Camber Leading Edge Device Design Methodology,’’ In: Proceedings of AIAA 5th ATIO and 16th Lighter-Than-Air Sys Tech. and Balloon Systems Conferences, 28 September, Arlington, VA, AIAA 2005- 7356.

[13] Kota, S., Ervin, G., Osborn, R. and Ormiston, R.A. 2008. ‘‘Design and Fabrication of an Adaptive Leading Edge Rotor Blade,’’ In: Proceedings of American Helicopter Society 64th Annual Forum, 29 April-1 May, Montreal, Canada (9 pp).

[14] Kota, S., Osborn, R., Ervin, G., Maric, D., Flick, P. and Paul, D.‘ 2009. ‘‘Mission Adaptive Compliant Wing - Design, Fabrication and Flight Test,’’ In: RTO Applied Vehicle Technology Panel (AVT) Symposium, Evora, Portugal, RTO-MP-AVT-168.

[15] Alessandro De Gaspari and Sergio Ricci. “Knowledge-based shape optimization of morphing wing for more efficient aircraft”. *International Journal of Aerospace Engineering*, 2015, 325724:1 – 19, 2015. doi: 10.1155/2015/325724.

[16] Alessandro De Gaspari and Sergio Ricci. A two–level approach for the optimal design of morphing wings based on compliant structures. *Journal of Intelligent Material Systems and Structures*, 22(10):1091–1111, 2011. doi: 10.1177/1045389X11409081.

[17] G. Diodati, A. Concilio, S. Ricci, A. De Gaspari, F. Huvelin, A. Dumont, and J. Godard. “Estimated performances of an adaptive trailing edge device aimed at reducing fuel consumption on a medium–size aircraft”. In *Industrial and Commercial Applications of Smart Structures Technologies (SPIE 2013)*, volume 8690, SPIE, pages 1 – 16, San Diego, CA, USA, 29 March 2013. Kevin M. Farinholt (Ed.). ISBN 9780819494733. doi: 10.1117/12.2013685.

[18] Mark Drela. “A User’s Guide to MSES 3.05”. MIT - Department of Aeronautics and Astronautics. July 2007. http://web.mit.edu/drela/Public/web/mses/mses.pdf

[19] L. Cambier, S. Heib, S. Plot: “The Onera elsA CFD software: input from research and feedback from industry”. *Mechanics & Industry*, Volume 14(N°3), 2013. Pages 159-174.

[20] C. Benoit, S. Péron, S. Landier: “Cassiopee: a CFD pre-and post-processing tool” , *Aerospace Science & Technology*, vol 45, pp. 275-283, 2015.

[21] S. Vasista, A. De Gaspari, S. Ricci, J. Riemenschneider, H.P. Monner, and B. van de Kamp. « Compliant structures–based wing and wingtip morphing devices”. *Aircraft Engineering and Aerospace Technology*, 88(2):311 – 330, 2016. doi: 10.1108/AEAT-02-2015-0067.

[22] Alessandro De Gaspari and Sergio Ricci. Application of the active camber morphing concept based on compliant structures to a regional aircraft. In *Industrial and Commercial Applications of Smart Structures Technologies (SPIE 2014)*, volume 9059, SPIE, pages 1 – 21, San Diego, CA, USA, 9 March 2014. K. M. Farinholt, S. F. Griffin (Eds.). ISBN 9780819499851. doi: 10.1117/12.2045225.

[23] Ghiringhelli, G. L., Masarati, P., and Mantegazza, P., “Multibody Implementation of Finite Volume C0 Beams", *AIAA Journal*, Vol. 38, No. 1, 2000, pp. 131-138.

[24] Miller, S., Vio, G. A., Cooper, J. E., Vale, J., da Luz, L., Gomes, A., Lau, F., Suleman, A., Cavagna, L., De Gaspari, A., Ricci, S., Riccobene, L., Scotti, A., and Terraneo, M., “SMorph - Smart Aircraft Morphing Technologies Project”, 51th AIAA/ASME/ASCE/AHS/ASC Structures, Structural Dynamics and Materials (SDM) Conference, AIAA 2010-2742, Orlando, Florida, 2010, pp. 1-14. doi: 10.2514/6.2010-2742.